Application of Mean-Force Potential Lattice Element Method to Modeling Complex Structures

Shayan Razi^a, Xuejing Wang^a, Navid Mehreganian^a, Mazdak Tootkaboni^{a,*} and Arghavan Louhghalam^{a,*}

^aDepartment of Civil and Environmental Engineering, University of Massachusetts, Dartmouth, MA, USA

ARTICLE INFO

Keywords:

Infrastructure Resilience

Energy-based modeling

Lattice element method

Mean-force potential

Calibrated interaction potentials

ABSTRACT

Natural hazards such as windstorms, earthquakes, and floods cause damage and failure to both structural and non-structural elements, significantly impacting the functional integrity and overall performance of the building systems. The economic loss due to such events and the often tortuous path to recovery call for revisiting engineering approaches to resilience assessment through developing simulation methods that provide a balance between fidelity and efficiency, particularly if the post-event assessment is to be performed at a large scale, e.g., the scale of a community. In this paper, we develop a discrete simulation framework for modeling the response of structures as a middle-ground solution between overly simplistic multi-degree-of-freedom models on the one hand and intricate FE models on the other. The framework draws upon the Potential-of-Mean-Force (PMF) approach to Lattice Element Method (LEM) where the main idea is to discretize the system into a set of particles that interact with each other through prescribed interaction potentials. These potentials are calibrated beforehand at member scale, for different structural and non-structural components. Here we focus on providing the main elements and the steps necessary for adaptation to modeling structural components in linear regime and leave the extension to nonlinear regime and the modeling of damage for future developments. This includes calibration of the potentials for structural members of different types (1D vs. 2D) under different actions (axial, bending, in-plane and out-of-plane actions) through an energetic handshake between the lattice model and continuum theories, e.g., the Timoshenko beam theory and Kirchhoff-Love plate theory. We explore the utility of the proposed method through its application to simulation of a set of building systems with different levels of complexity and under various loading conditions.

1. Introduction

The vulnerability of U.S. civil infrastructures to natural hazards such as windstorms, earthquakes, and flooding and their severe economic and societal impacts are well known. In 2020 alone, the total damage from natural disasters amounted to \$95 billion in loss [1]. These widespread impacts, followed by the lengthy and costly recovery processes, call for novel, robust, and efficient damage assessment tools for resilience analytics that allow for accurate examination of functional integrity for structures with various levels of complexity. The corresponding extreme loading conditions can cause failure and damage to both structural and non-structural elements, leading to loss of functionality of the entire structural system. Despite the proven fact that failure of non-structural members can significantly contribute to the overall performance under extreme loading conditions [2, 3, 4, 5, 6], many existing approaches to damage assessment, consider solely the failure of structural components and disregard the role of non-structural elements, such as non-load-bearing walls, partitions, and building envelop, on system's functional integrity, a practice that can prove detrimental to the assessment process considering the impact of sever damage in these non-structural elements on system's overall performance [7, 8].

Disregarding the impact of non-structural failure on system-level performance is mostly rooted in the substantial computational expense associated with the detailed modeling of the system at all levels. The research efforts, to a

Email addresses: mtootkaboni@umassd.edu (M. Tootkaboni); alouhghalam@umassd.edu (A. Louhghalam) ORCID(s):

^{*}Corresponding author

large extent, have focused on developing rigorous nonlinear models to investigate the performance of non-structural components as they interact with structural members. These include detailed finite element simulations of the elements and connections [9] and development and use of special nonlinear elements (e.g., macro-element-based models in OpenSees [10]) among others [11, 12, 13, 14]. While such approaches to modeling can accurately capture the interaction and load transfer between structural and non-structural elements, they require significant computational resources and are not amenable to large-scale system/community level analysis.

Additionally, most simulation strategies rely on continuum approaches and, as such, are not robust against modeling discontinuity, failure, and damage. Finite element method, for example, has been extensively used for modeling fracture in continuum domains with different types of pre-existing discontinuity [15, 16, 17]. One of the challenges associated with such strategies is that they require mesh refinement around discontinuities to conform to the geometry during crack propagation [18, 19]. While more advanced methods such as the extended-finite element method (XFEM) have been developed by elemental enrichment of FEM to minimize the need for re-meshing around discontinuities and complex morphologies [20, 21, 22, 23], there still remain unresolved issues when modeling non-linear failure [24, 25, 26] or dynamic fracture [25, 27, 28], particularly if the goal is to perform simulation-based assessments at large scales, say the scale of a community.

Discrete methods have recently become increasingly popular in modeling materials at the meso-scale due to their inherent capability and effectiveness in simulating a variety of material behaviours, and complex failure and fracture phenomena [29, 30, 31, 32, 33, 34]. These include distinct or discrete element method (DEM) [35], widely used methods for simulating granular materials, rock mechanics and more recently architected materials [36, 37, 38, 39], material point method (MPM) [40], a powerful tool for simulating the crack initiation and growth under dynamic loading conditions for brittle and ductile materials [41, 42], rigid block spring method (RBSM) [43], used for simulation of cement-based and other cohesive materials [44, 45], among others.

Lattice Element Method (LEM) is a class of discrete methods that has proved very effective in robustly modeling fracture, crack propagation and coalescence of discontinuities in quasi-brittle and heterogeneous materials [46, 47, 48, 49]. The core idea of the method is to discretize the material domain into a number of particles connected via one-dimensional elements that break according to strength- or strain-based failure criteria [50, 51, 52]. LEM has been used for modeling microcracks in single-phase or multi-phase materials [53], as well as crack formation, debonding, and crack propagation in concrete at the meso-scale [54, 55, 56, 57]. There have also been efforts to utilize LEM for examination of the energy dissipation during failure through the definition of element-level softening models [58].

A potential of mean force (PMF) approach to LEM has recently been proposed that uses interaction potentials, akin to those used in molecular simulations, to capture the interactions between material points in the discretized domain [59]. A similar approach to free-energy calculation has been successfully used as an efficient upscaling strategy from molecular scale to meso-scale in multi-scale modeling of complex materials such as cement [60], and clay and soil [61], among others. The PMF-based LEM allows for direct implementation of energetic definition of fracture as a successive irreversible process of energy release due to bond breakage between a sequence of thermodynamic equilibrium states [59, 62]. More recently, Wang et al. [63] proposed a novel hybrid methodology for simulating the fracture of heterogeneous materials. The proposed methodology transcends conventional LEM by enabling near-global enforcement of the Griffith criteria at a significantly reduced computational cost.

In this study, we leverage the PMF approach to LEM and adapt it to develop a novel tool for modeling the response of building systems. We do this based on the premise that the PMF approach to LEM offers several advantages regarding the potential for the examination of a building system's overall performance and functional integrity, namely, (i) a handshake between computational efficiency and fidelity, allowing for the modeling of the entire system comprised of both structural and non-structural components. We view this as finding the middle ground between overly simplistic multi-degree-of-freedom models [64, 65] and intricate FE models for the case where the analysis needs to be performed at a massive scale, e.g., the scale of a community, (ii) the discrete nature of the lattice element method that permits proper modeling of failure and damage without confronting the discontinuity and instability challenges intrinsic to continuum approaches, (iii) the prospects of leveraging a broad range of effective interaction potentials to enable the modeling of different nonlinear behaviors in structural and nonstructural members [66, 59, 67, 68, 69, 30], along with energy-based failure criteria [70, 71, 72]. Having laid out the utilities offered by the PMF approach to LEM, however, we note that this study is focused on providing the elements of the conceptual framework and its application in linear regime and, as such, leaves the extension to nonlinear regime and the modeling of damage for future. Furthermore, with

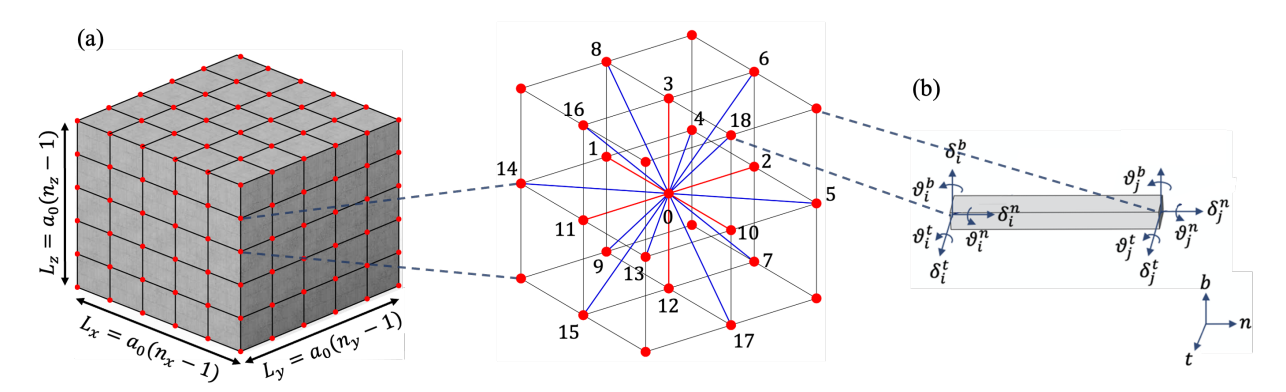


Figure 1: (a) Discretization of a solid medium with the lattice of unit cell size a_0 ; n_x , n_y and n_z are the number of nodes along the axes x, y and z; each particle is connected to its 18 immediate neighboring particles; (b) Translational, $\vec{\delta}_i = \{\delta_i^n, \delta_i^b, \delta_i^t\}$, and rotational, $\vec{\theta}_i = \{\theta_i^n, \theta_i^b, \theta_i^t\}$, degrees of freedom in the bond's local coordinate system with unit vectors $[\vec{e}_n, \vec{e}_h, \vec{e}_t]$.

the assumption of quasi-static conditions, the current formulation of LEM is not amenable to modeling the dynamic response of systems. While our ongoing research focuses on leveraging advances in MD simulation techniques [73, 74] and enabling LEM to traverse the dynamic equilibrium path, the developments in this manuscript are solely for quasi-static conditions and establish the basis for further extensions.

The organization of the paper is as follows: We first review the PMF approach to LEM in Section 2. The details pertaining to the adaptation of LEM to model structural elements are presented in Section 3. These include the calibration of harmonic interaction potentials for one- and two-dimensional elements under both in-plane and out-of-plane actions through an energetic handshake between the continuum theories, that is the Timoshenko beam theory and Kirchhoff- Love plate theory, and the lattice model, as well as the validation of the simulation results. In Section 4 we showcase the application of the proposed approach to different structures, from a plate under combined loading to more complicated scenarios, including the modeling of an entire building comprised of beams, columns, floors and a central core. Section 5, finally, provides the concluding remarks.

2. Lattice Element Method: A Potential-of-Mean-Force Approach

The main premise in the potential-of-mean-force (PMF) approach to the Lattice Element Method (LEM) is the ability to describe the mechanical behavior of a medium by discretizing it into particles that interact with each other through interaction potentials [62]. The total internal energy of the system comprised of N particles is then the summation of the particles' ground-state energy and the interaction energy between the particles:

$$U_{tot} = \sum_{i}^{N} U_{i}(\vec{x}_{i}) + \sum_{i,j}^{N} U_{ij}(\vec{x}_{i}, \vec{x}_{j}) + \sum_{i,j,k}^{N} U_{ijk}(\vec{x}_{i}, \vec{x}_{j}, \vec{x}_{k}) + ...,$$
(1)

where \vec{x}_i denotes the position vector of *i*th particle, and U_i , U_{ij} and U_{ijk} are respectively the ground-state, twoand three-body interaction energies [62]. The PMF approach is consistent with the classical LEM, when only twoand three-body interactions between a point and its nearest neighbors are accounted for and the higher-order terms are disregarded. In the classical LEM, the interactions between material points are modeled via axial, bending, and occasionally shear and torsional actions [75, 76, 77, 50] and the total internal energy of the system reads:

$$U_{tot} \approx \frac{1}{2} \sum_{i=1}^{N} \sum_{j \in I_i} -\epsilon_{ij}^0 + U_{ij}^S(\vec{\theta}_i, \vec{\theta}_j) + U_{ij}^B(\vec{\theta}_i, \vec{\theta}_j) + U_{ij}^T(\vec{\theta}_i, \vec{\theta}_j), \tag{2}$$

where I_i denotes a set including 18 immediate neighbors of the i^{th} particle according to the lattice configuration illustrated in Fig. 1, and $\vec{\theta}_i = (\vec{\delta}_i, \vec{\vartheta}_i)$ is the corresponding generalized vector of degrees of freedom. Here $\vec{\delta}_i =$

 $\{\delta_i^n, \delta_i^b, \delta_i^t\}$ and $\vec{\vartheta}_i = \{\vartheta_i^n, \vartheta_i^b, \vartheta_i^t\}$ respectively denote vectors of translational and rotational degrees of freedom in the local lattice coordinate with unit vectors $[\vec{e_n}, \vec{e_b}, \vec{e_t}]$; see Fig. 1(b). Finally, U_{ij}^S , U_{ij}^B and U_{ij}^T represent the energy contributions from stretch, bending and torsional actions, respectively, for the bond connecting particles i and j with a well depth energy of ϵ_{ij}^0 . The translational and rotational degrees of freedom at each equilibrium state is then determined via minimizing the total potential energy of the system according to the minimum potential energy theorem:

$$\{\vec{\theta}_{1}, ..., \vec{\theta}_{N}\} = \operatorname{argmin}_{\vec{\theta}_{1}, ..., \vec{\theta}_{N}} U_{tot}(\vec{\theta}_{1}, ..., \vec{\theta}_{N}) - W(\vec{\theta}_{1}, ..., \vec{\theta}_{N})$$
(3)

with W denoting the external work supplied to the system. Hence, the forces and moments in the bonds, i.e. the derivatives of the internal energy with respect to the corresponding degrees of freedom:

$$\vec{F}_{i}^{j} = -\frac{\partial U_{tot}}{\partial \vec{\delta}_{i}}; \qquad \vec{M}_{i}^{j} = -\frac{\partial U_{tot}}{\partial \vec{\theta}_{i}}, \tag{4}$$

satisfy the balance of momentum:

$$\vec{F}_i^j + \vec{F}_j^i = \vec{0}; \qquad \vec{M}_i^j + \vec{M}_j^i + (\vec{x}_j - \vec{x}_i) \times \vec{F}_j^i = \vec{0}. \tag{5}$$

With LEM inherently a force-field method, the stress components at particle i –as a continuum metric– are determined a posteriori via the virial expression [78]:

$$\sigma_i = \frac{1}{2v_i} \sum_{j \in I_i} (\vec{x}_j - \vec{x}_i) \otimes \vec{F}_i^j. \tag{6}$$

with v_i the voxel volume centered at particle i, and \otimes representing the tensor product.

The PMF approach enables LEM to leverage a wide range of interaction potentials for characterizing different behaviors of structural and non-structural members. Focusing on the linear response and the harmonic potential, the internal energy of a bond connecting particles i and j is decomposed into the components associated with stretch (U_{ij}^S) , bending $(U_{ij}^{B,b})$ and $U_{ij}^{B,t}$ corresponding to local axes b and t), and torsional (U_{ij}^T) actions:

$$U_{ij}^{S} = \frac{1}{2} \epsilon_{ij}^{S} (\lambda_{ij}^{n})^{2},$$

$$U_{ij}^{B,t} = \frac{1}{2} \epsilon_{ij}^{B,t} \left\{ (\lambda_{ij}^{b} - \vartheta_{i}^{t})^{2} + (\lambda_{ij}^{b} - \vartheta_{i}^{t}) (\vartheta_{i}^{t} - \vartheta_{j}^{t}) + \frac{1}{3} (\vartheta_{i}^{t} - \vartheta_{j}^{t})^{2} \right\} + \frac{1}{2} \hat{\epsilon}_{ij}^{B,t} (\vartheta_{j}^{t} - \vartheta_{i}^{t})^{2},$$

$$U_{ij}^{B,b} = \frac{1}{2} \epsilon_{ij}^{B,b} \left\{ (\lambda_{ij}^{t} + \vartheta_{i}^{b})^{2} + (\lambda_{ij}^{t} - \vartheta_{i}^{b}) (\vartheta_{j}^{b} - \vartheta_{i}^{b}) + \frac{1}{3} (\vartheta_{j}^{b} - \vartheta_{i}^{b})^{2} \right\} + \frac{1}{2} \hat{\epsilon}_{ij}^{B,b} (\vartheta_{j}^{b} - \vartheta_{i}^{b})^{2},$$

$$U_{ij}^{T} = \frac{1}{2} \epsilon_{ij}^{T} (\vartheta_{j}^{n} - \vartheta_{i}^{n})^{2},$$

$$(7)$$

where $\vec{\lambda}_{ij} = (\vec{\delta}_j - \vec{\delta}_i)/l_{ij}^0$ is the normal strain, $l_{ij}^0 = |(\vec{x}_j - \vec{x}_i).\vec{e}_n|$ denotes the bond initial length, whereas ϵ_{ij}^S , ϵ_{ij}^T are, respectively, the non-negative parameters corresponding to interaction potentials for stretch, torsion, and bending in two directions. Modeling a structural system with reasonable fidelity requires a discretization of the structural domain with high-resolution leading to "short" and "deep" bonds for which the shear effect is non-negligible. We thus define additional potential parameters $\hat{\epsilon}_{ij}^{B,t}$ and $\hat{\epsilon}_{ij}^{B,b}$ and modify the bending energy expressions to account for the contribution of shear deformation to the total internal energy expression. The above representation of the bond's internal energy can also be presented as the following quadratic expression:

$$U_{ij}(\vec{\theta}_i, \vec{\theta}_j) = \frac{1}{2} \begin{pmatrix} \vec{\theta}_i \\ \vec{\theta}_j \end{pmatrix}^T K_{ij} \begin{pmatrix} \vec{\theta}_i \\ \vec{\theta}_j \end{pmatrix}, \tag{8}$$

where K_{ij} , the stiffness matrix for link ij (see Appendix I), accounts for the stretch, bending, shear, and torsional actions.

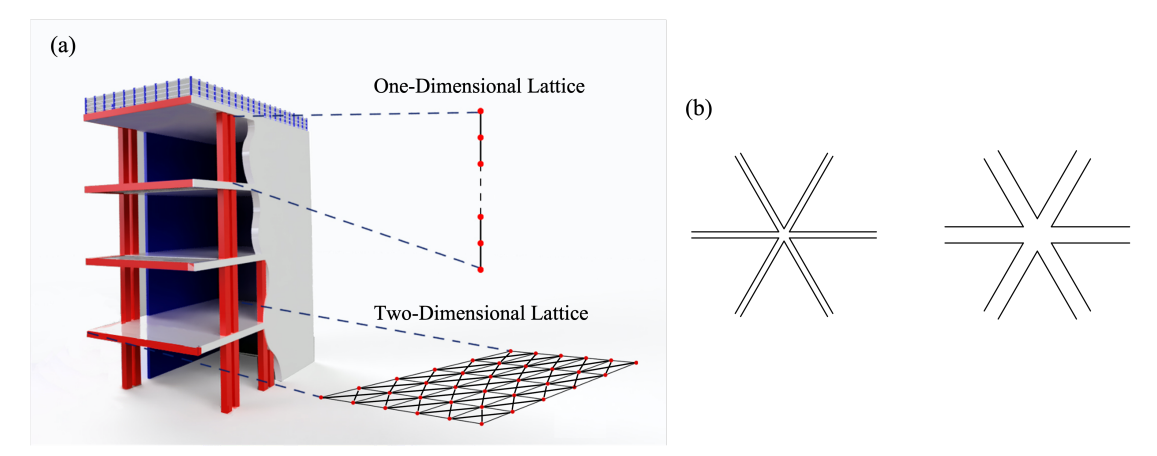


Figure 2: (a) Lattice discretization of a building into one-dimensional (1D) and two-dimensional (2D) members; (b) A material point in the lattice system is connected to its neighboring points through two different types of 1D elements: the slender element (left) and the deep element where shear deformation is significant (right).

Since the conception of lattice element method, its use has been mainly limited to modeling material systems where the domain is discretized via a lattice-like network of particles connected via interaction potentials. The parameters of the interaction potentials are calibrated so as to describe three-dimensional or, in some cases, in-plane response of the material. Buildings and structural systems, however, are composed of one-dimensional (e.g., beams, columns, braces, etc.) and two-dimensional (e.g., floors, partitions, building envelope, etc.) members. In what follows, we adapt LEM to simulate the response of both types of structural members and subsequently an entire building system.

3. Adaptation to Structural Elements: Calibration of Potential Parameters

Structural elements, whether 1D or 2D, are discretized by a lattice network (see Fig. 2(a)) with nodes exhibiting both displacement and rotational degrees of freedom and the interaction between the nodes modeled via harmonic energy potentials. The non-negative parameters of the interaction potentials are then calibrated so as to simulate the behavior of different structural members.

3.1. One-dimensional members

The parameters of the interaction potential for one-dimensional (1D) elements are readily calibrated through a handshake between the total energy of the lattice in LEM, assuming harmonic interaction potentials, and the strain energy of the 1D elements due to stretch, bending, torsion, and shear. We note that a high-resolution discretization that allows for a more accurate simulation can result in short and deep 1D elements where shear deformation and its contribution to internal energy are significant; see Fig. 2(b) for a material point connected to its neighboring points in a 2D lattice. To account for this, we use the Timoshenko beam theory in the calibration process of 1D elements. More specifically, to obtain the parameters of the interaction potentials, the total internal energy in Eq. (2) for a member discretized into n particles is set equal to the total internal energy of the same member under axial, bending and shear actions.

The results are summarized in Table 1 in terms of the elastic and geometric properties of the 1D element. Here $\Phi^{b,t} = 12EI^{b,t}/(GAl_{ij}^{0.2})$ is a dimensionless number describing the bending to shear stiffness ratio, E, G and v are respectively the elastic modulus, shear modulus and Poisson's ratio of the material, whereas A, I and J are the area, second moment of inertia and torsional constant of the member's cross-section. It is readily seen from the results that the potential parameters for 1D elements are independent of the level of discretization n.

3.2. Two-dimensional members

Two-dimensional (2D) components appear in both structural (e.g., shear walls, floors, bearing walls) and non-structural (e.g., partitions and building envelope) members when simulating buildings as systems. Fig. 3 shows a 2D plate of dimensions l_x , l_y and thickness d discretized via a regular 2D lattice. Each particle interacts with a maximum of eight neighboring particles across straight and diagonal directions. Akin to the classical plate theory, the interactions

ϵ_{ij}^S	$\epsilon_{ij}^{B,(b,t)}$	$\hat{\epsilon}_{ij}^{B,(b,t)}$	ϵ_{ij}^T
EAl^0_{ij}	$\frac{12EI^{b,t}}{l_{ij}^0(\phi^{b,t^*}+1)}$	$\frac{EI^{b,t}\phi^{b,t}}{2l_{ij}^0(\phi^{b,t}+1)}$	$rac{GJ}{l_{ij}^0}$

Table 1: Calibrated potential parameters for one-dimensional member

between particles are decomposed into membrane (in-plane) and flexural (out-of-plane) actions. The corresponding potential parameters are then calibrated according to the plane stress and Kirchhoff-Love theories, respectively.

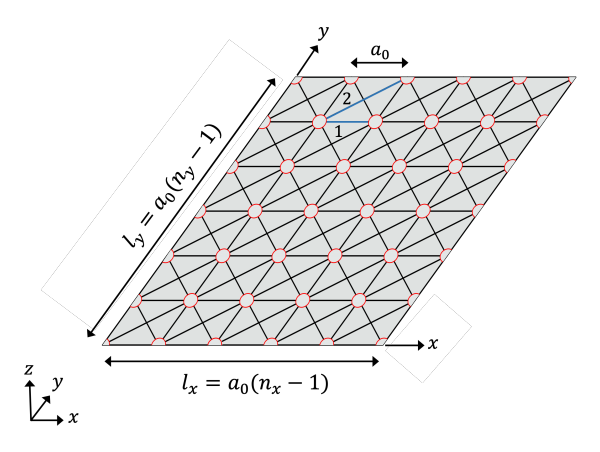


Figure 3: Lattice discretization of a 2D plate of dimensions l_x , l_y with lattice size a_0 . Within this lattice configuration, each particle interacts with up to eight neighboring particles across the straight bonds connecting points in x and y directions and the diagonal bonds connecting points in the diagonal directions, denoted by 1 and 2 respectively.

3.2.1. In-plane calibration

Consider an isotropic and homogeneous membrane in plane stress condition discretized into $n_x \times n_y$ points using a 2D lattice as shown in Fig. 3. The lattice is composed of two types of bonds, the short bonds connecting points in x and y directions and the long bonds connecting points in the diagonal directions. Noting that the length of a bond plays a key role in its internal energy, we require four unique potential parameters to characterize the in-plane response of the lattice. These parameters are associated with stretch e_1^S , e_2^S and in-plane bending $e_1^{B,b}$ and $e_2^{B,b}$ actions, with subscripts 1 and 2, respectively, representing the parameters corresponding to the closest neighbor direction ($l_{ij}^0 = a_0$) and the direction of neighbors along the diagonal ($l_{ij}^0 = \sqrt{2}a_0$).

To calibrate the parameters of the interaction potential, we leverage the theory of minimum potential energy, stating that the deformations and rotations of all degrees of freedom at equilibrium must minimize the total potential energy of the medium. It is also known that the components of the elastic stiffness matrix are the second derivatives of internal energy density with respect to the corresponding strain and rotational components:

$$C_{ij} = \frac{1}{(n_x - 1)(n_y - 1)a_0^2} \frac{\partial^2 U_{tot}}{\partial \varepsilon_i \partial \varepsilon_j}, \qquad i, j = 1, 2, 4$$

$$(9)$$

with ε_1 and ε_2 the in-plane normal strains in x and y directions, and ε_4 the in-plane shear strain. We thus subject the 2D lattice to an in-plane uniform strain field, characterized via a vector of strains $\vec{\varepsilon} = \left[\varepsilon_1, \varepsilon_2, \varepsilon_4\right]^T$. Removing the subscripts i and j for notational simplicity, the normalized in-plane deformations at each lattice bond reads:

$$\lambda^n = O^n \vec{\epsilon}, \quad \lambda^l = O^l \vec{\epsilon}$$
 (10)

Here $\vec{\epsilon}$ is the applied strain, and Q^n and Q^t are matrices of transformation from the global to the lattice local system of coordinates given in Appendix II. Utilizing Eqns. (2), (7), and (10), the total energy of the system is expressed as a function of the four unique energy parameters (ϵ_1^S , ϵ_2^S , $\epsilon_1^{B,b}$ and $\epsilon_2^{B,b}$). Finally, the potential parameters are determined by equating the second derivatives of the total energy and the corresponding components of the plane stress stiffness matrix for isotropic materials:

$$\begin{bmatrix} C_{11} \\ C_{12} \\ C_{44} \end{bmatrix} = \frac{E}{1 - v^2} \begin{bmatrix} 1 \\ v \\ (1 - v)/2 \end{bmatrix} = \frac{1}{a_0^2} \begin{bmatrix} n/(n-1) & 1/2 & 0 & 1/2 \\ 0 & 1/2 & 0 & -1/2 \\ 0 & 1/2 & n/2(n-1) & 1/2 \end{bmatrix} \begin{bmatrix} \epsilon_1^S \\ \epsilon_2^S \\ \epsilon_1^B \\ \epsilon_2^B \end{bmatrix}, \tag{11}$$

The results are summarized in Table 2 in terms of material properties (elastic modulus E, Poisson's ratio v), lattice configuration properties (level of discretization n, size of the lattice unit cell a_0), and plate thickness d. As can be seen, the lattice model adopted will reduce to the classical central-force lattice when the parameter associated with in-plane bending internal energy $\epsilon_i^{B,b}$ is equal to zero, leading to a lattice representative of an isotropic membrane with a Poisson's ratio v=1/3 [62]. Nonzero values of $\epsilon_i^{B,b}$, on the other hand, enable the lattice with both axial and bending actions to model membranes with a wide range of Poisson's ratios. The limits of Poisson's ratio are governed by the non-negativeness of the parameters of interaction potentials. Within the limits defined by this constraint, the harmonic potentials in Eq. (7) require three nonzero energy parameters to properly simulate the isotropic behavior of a membrane by the lattice system shown in Fig. 3.

Energy parameters	$-1 < \nu \le 0$	$0 \le \nu \le 1/3$
ϵ_1^S	$\frac{E(n-1)}{n(1-\nu)}a_0^2d$	$\frac{E(n-1)}{n(1+\nu)}a_0^2d$
ϵ_2^S	0	$\frac{2Ev}{1-v^2}a_0^2d$
$\epsilon_1^{B,b}$	$\frac{E(n-1)}{n(1-\nu)}a_0^2d$	$\frac{E(1-3\nu)(n-1)}{n(1-\nu^2)}a_0^2d$
$\epsilon_2^{B,b}$	$\frac{2Ev}{v^2-1}a_0^2d$	0

Table 2: Calibrated potnatial parameters for in-plane deformation

The calibrated potential parameters in Table 2 are validated by comparing the analytical values for dimensionless stiffness constants C_{11}/E , C_{12}/E and C_{44}/E with those obtained from numerical simulations of the discretized system. The results are illustrated in Fig. 4 for a wide range of Poisson's ratio ν and different levels of discretization n. We observe that, especially for positive Poisson's ratio, a relatively low-resolution discretization with LEM can provide results that are in close agreement with their continuum counterparts.

3.2.2. Out-of-plane calibration

We postulate that the out-of-plane deformation of the lattice system is a consequence of torsional and out-of-plane bending actions. We hence use the Kirchhoff-Love plate theory to calibrate the parameters corresponding to the torsion ϵ^T and out-of-plane bending $\epsilon^{B,t}$ potentials. Analogous to the in-plane calibration procedure, we identify four unique potential parameters, $\epsilon_1^{B,t}$, $\epsilon_2^{B,t}$, ϵ_1^T and ϵ_2^T , with subscripts 1 and 2, respectively, corresponding to short bonds $l_{ij}^0 = a_0$ and the diagonal bonds $l_{ij}^0 = \sqrt{2}a_0$.

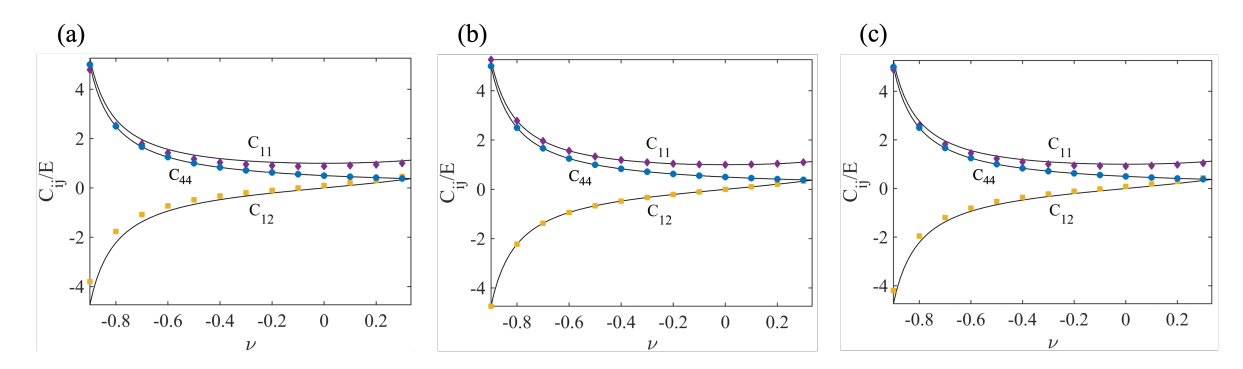


Figure 4: Validation of the in-plane calibration procedure through comparing theoretical values of dimensionless stiffness constants C_{11}/E , C_{12}/E and C_{44}/E (solid lines) in terms of Poisson's ratio with those obtained by numerical simulations of discretized lattice system (symbols) for different levels of discretization n; (a) n = 5; (b) n = 11; (c) n = 21. The results indicate a close match between the calibrated lattice discretized system and its continuum counterparts at relatively low-resolutions.

The out-of-plane deformation of a plate, according to the Kirchhoff-Love theory is described using the moment-curvature relationships:

$$\begin{bmatrix} M_{x} \\ M_{y} \\ M_{xy} \end{bmatrix} = \mathbf{F} \begin{bmatrix} \kappa_{x} \\ \kappa_{y} \\ \kappa_{xy} \end{bmatrix} \tag{12}$$

where M_x and M_y represent the moment around x and y axes, and M_{xy} is the twisting moment. The corresponding curvatures are $\kappa_x = \partial^2 w/\partial x^2$, $\kappa_y = \partial^2 w/\partial y^2$, $\kappa_{xy} = \partial^2 w/\partial x \partial y$, and the flexural rigidity matrix is given by:

$$\mathbf{F} = D \begin{bmatrix} 1.0 & v & 0 \\ v & 1.0 & 0 \\ 0 & 0 & 2(1-v) \end{bmatrix}, \quad D = \frac{Ed^3}{12(1-v^2)}$$
 (13)

with d the plate thickness. It follows that the components of the flexural rigidity matrix are the second derivatives of the strain energy density due to out-of-plane deformation with respect to curvatures:

$$F_{ij} = \frac{1}{(n_x - 1)(n_y - 1)a_0^2} \frac{\partial^2 U_{tot}}{\partial \kappa_i \partial \kappa_j}$$
(14)

To calibrate the out-of-plane potential parameters, we subject the lattice to deformation fields that result in bending of the plate with a constant curvature. The total energy of the lattice system is a function of the curvatures κ_x , κ_y , κ_{xy} and the out-of-plane rotations θ^n , θ^t . To obtain the four unique parameters of the interaction potential, the second derivatives of the energy with respect to the curvatures are then set equal to the corresponding components of the flexural rigidity matrix of a thin isotropic plate. Table 3 summarizes the corresponding potential parameters for both straight and diagonal bonds.

The dimensionless components of the flexural rigidity matrix F_{ij} for the calibrated lattice are compared with the ones from Kirchhoff-Love plate theory in Fig. 5 indicating a close agreement for a wide range of Poisson's ratio and different levels of discretization. We, however, observe that a higher resolution is required for convergence compared to the in-plane calibration, which can be attributed to the complexity of the out-of-plane bending deformation. Nevertheless, the convergence for positive values of Poisson's ratio is achieved with a rather low resolution discretization.

3.3. Additional validation for combined loading

By way of example, we use LEM with calibrated interaction potentials to model a plate of thickness 0.12m with elastic modulus E = 23.52 GPa and Poisson's ratio v = 0.2. The plate domain is discretized via a $n_x = 41$ by $n_y = 31$ lattice of size $a_0 = 0.2$ m, and is subjected to a general deformation field (see Fig. 6).

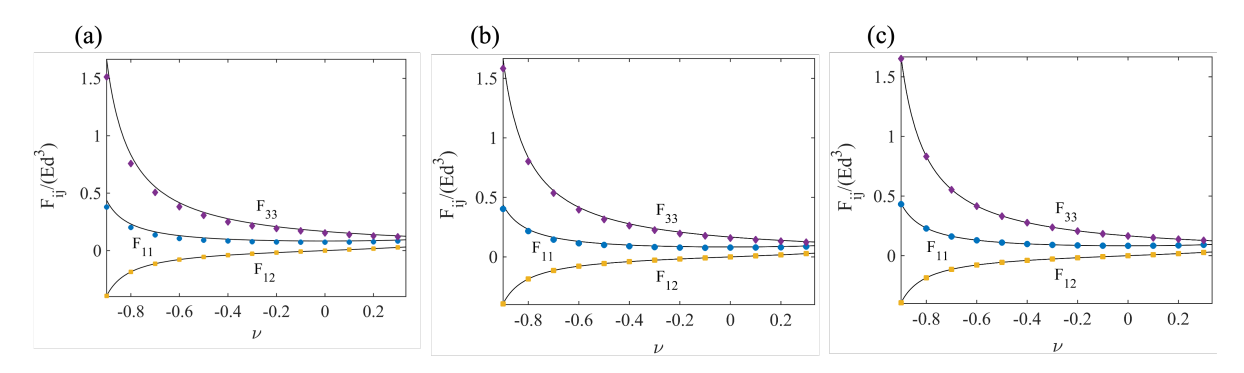


Figure 5: Validation of the out-of-plane calibration procedure through comparing the theoretical dimensionless flexural rigidity constants $F_{ij}/(Ed^3)$ (solid lines) as a function of Poisson's ratio with those obtained from numerical simulations of discretized lattice system (symbols) at different discretization levels n; (a) n = 21, (b) n = 51, and (c) n = 97. The results indicate that, in comparison to the in-plane response, a more resolved lattice discretization is needed to achieve accurate results. However, for positive values of Poisson's ratio of interest in structural mechanics applications, accurate results can be achieved at relatively low resolutions.

Energy parameters	$-1 < \nu \le 0$	$0 \le v \le 1/3$
$\epsilon_1^{B,t}$	$\frac{12D(n-1)(1+\nu)}{n}$	$\frac{12D(n-1)(1-\nu)}{n}$
$\epsilon_2^{B,t}$	0	12Dv
ϵ_1^T	$\frac{D(n-1)(1-\nu)}{n}$	$\frac{D(n-1)(1-3\nu)}{n}$
ϵ_2^T	-Dv	0

Table 3: Calibrated energy parameters describing out-of-plane deformation

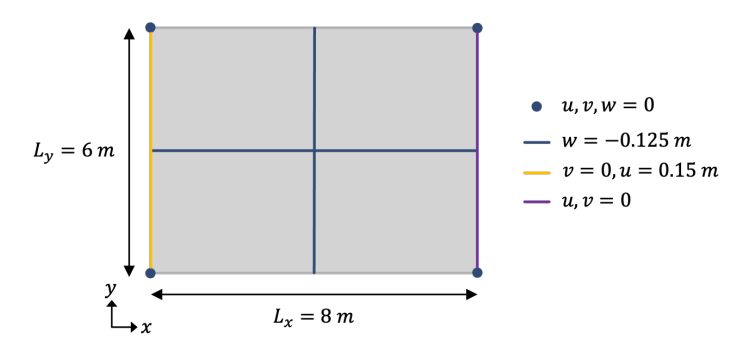


Figure 6: Geometry and boundary conditions for a concrete plate example with a thickness of 0.12m, elastic modulus of E = 23.52 GPa and Poisson's ratio of v = 0.2. The plate is subjected to a general deformation field, causing both in-plane and out-of-plane displacements.

The results in Fig. 7 indicate a close agreement between the displacements and rotations obtained via LEM and those from finite element analysis. The figures in the right column (7 c, f, i and l) display the probability density function

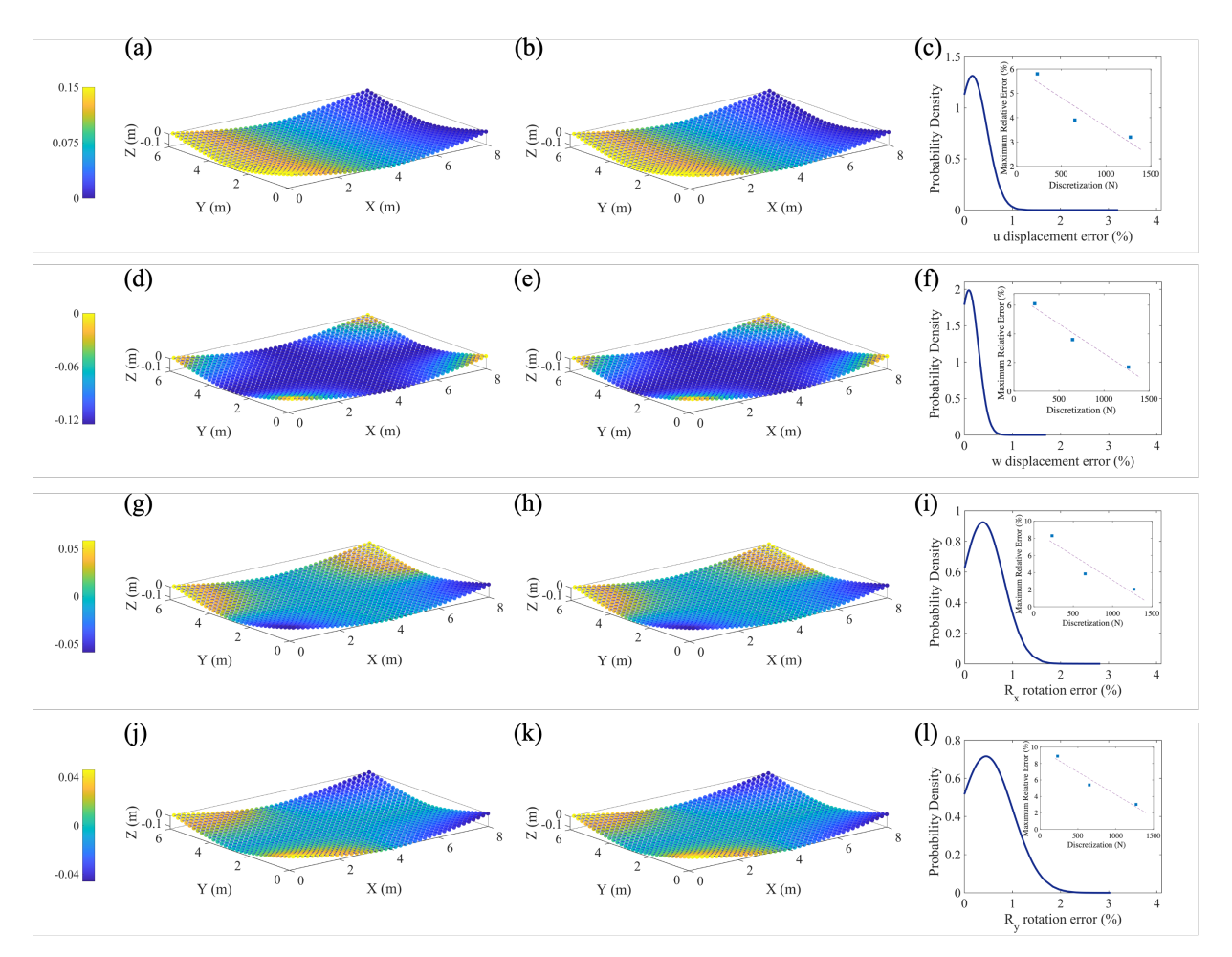


Figure 7: Comparison of the results of PMF-based LEM and finite element analysis for the plate problem depicted in Fig. 6 discretized by a lattice of size $a_0 = 0.2$ m. (a) and (b) display the in-plane deformation u in x direction, respectively, obtained via PMF-based LEM and FEM simulation, whereas (d) and (e) present the out-of-plane deformation w. Similar comparisons are presented for rotations around the x axis (R_x) in (g) and (h), and around the y axis (R_y) in (j) and (k). The right column (c,f,i,l) illustrates the probability density functions of the relative error for each of the above displacement components. Relative errors greater than 2% are only observed in a limited number of particles, indicating a close agreement with the result of FEM. The insets show the reduction of the maximum relative error with increasing resolution of discretization.

of the percentage relative error and the insets exhibit the decay of maximum error with increased resolution. As can be seen, errors higher than 2% are only observed for a small number of nodes and decline further by increasing the discretization resolution. The largest relative errors are generally attributed to insignificant values of the corresponding displacement components.

4. Application to Multi-story Building Systems

In this section, we simulate the response of different building systems using the PMF-based lattice element methods developed in the preceding sections. The systems under examination include: (i) a multi-story building made of moment-resisting frames in two directions and floor systems, (ii) a core system analogous to shear cores in buildings, and (iii) a multi-story building with moment-resisting frames, floor systems and an inner core. The above systems provide systems of different complexity comprised of both 1D and 2D members, allowing for a thorough examination of the utility of the proposed simulation framework in modeling the responses of the structures as well as the interactions

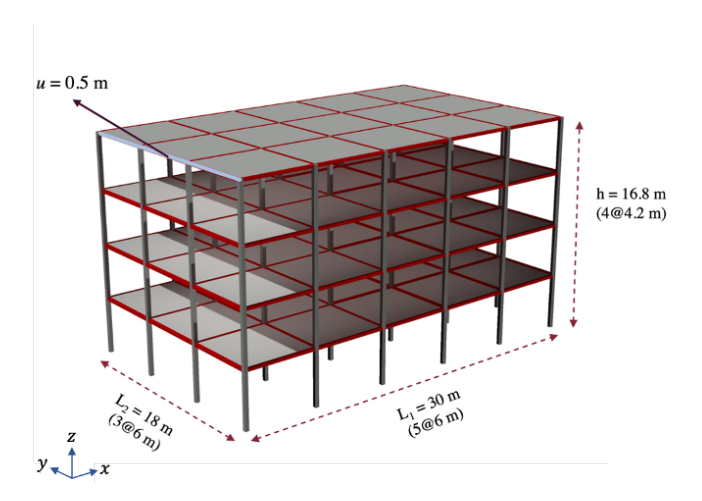


Figure 8: Schematic of the four-story concrete building, after the Department of Energy (DOE) reference building library for medium offices [79]. The structural system comprises moment-resisting frames in two directions with rigid connections, alongside floor systems and fixed supports. The building is subject to a lateral displacement of u = 0.5m (in the x direction) on the left side of the top floor.

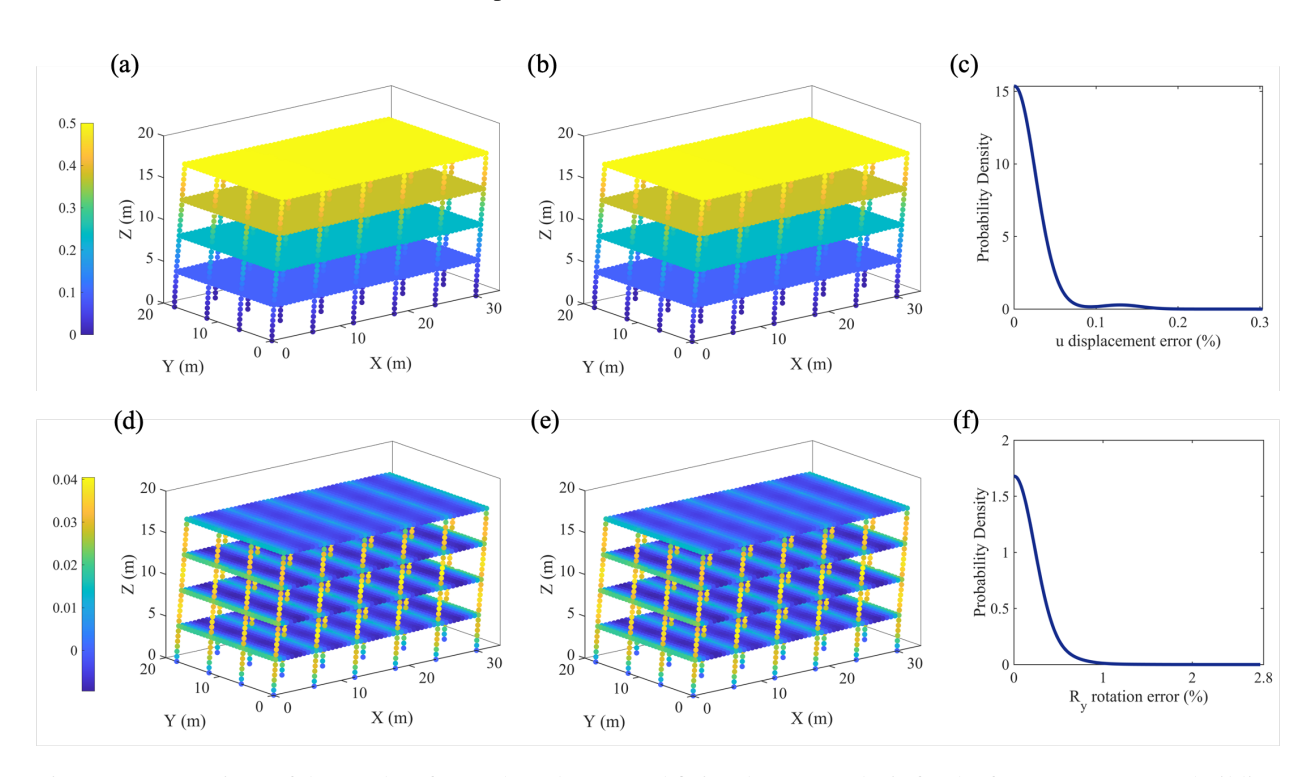


Figure 9: Comparison of the results of PMF-based LEM and finite element analysis for the four-story concrete building represented in Fig. 8 discretized by a lattice of size $a_0 = 0.3$ m. (a) and (b) represent displacement u in x direction obtained via PMF-based LEM and FEM simulations, respectively, whereas (d) and (e) illustrate the rotation around the y axis (R_y). Figures (c,f) illustrate the probability density functions of the relative error for u and u and u and rotation u and u a

between 1D and 2D members. For simplicity and without loss of generality, all 1D members (beams and columns) are assumed to have a square cross-section with a side length of 0.45m, and the thickness of 2D members (floors and roof)

is set at 0.12m. The material is considered to be linear elastic with Young's modulus E = 23.52 GPa and Poisson's ratio v = 0.2. Using the above material and geometric properties, the parameters of the interaction potentials for 1D and 2D members are determined according to the calibration procedure described in Section 3 and the robustness of the proposed framework is demonstrated via comparison of the results with those obtained from Finite Element Analysis.

4.1. Multi-story building

A 4-story building, resembling the Department of Energy (DOE) reference building library for medium offices [79], as illustrated in Fig. 8, is considered. The structure comprises moment-resisting frames in two directions with rigid connections, floor systems and fixed supports. The building is subject to a lateral displacement of u = 0.5m in x direction at the left side of the top floor, as shown in the figure, and is discretized via a lattice of size $a_0 = 0.3m$. A finite element model with the same resolution is used to provide a benchmark for comparison. Fig. 9 compares the displacement in x direction (u) and rotation around y axis (R_y) obtained via LEM and FEM. The right column in the figure shows the probability density function of the percentage relative error, with the 95-percentiles at 0.07% for the displacement u and 0.79% for the rotation R_y , both indicating a close agreement between the two methods. Similar to the plate example in Section 3.3 the maximum discrepancy between the two models pertains to the deformations with negligible magnitudes. For instance, the maximum relative error of 0.31% in displacement u and 2.76% in rotation R_y both occur in columns of the first storey, with the corresponding absolute values approaching zero.

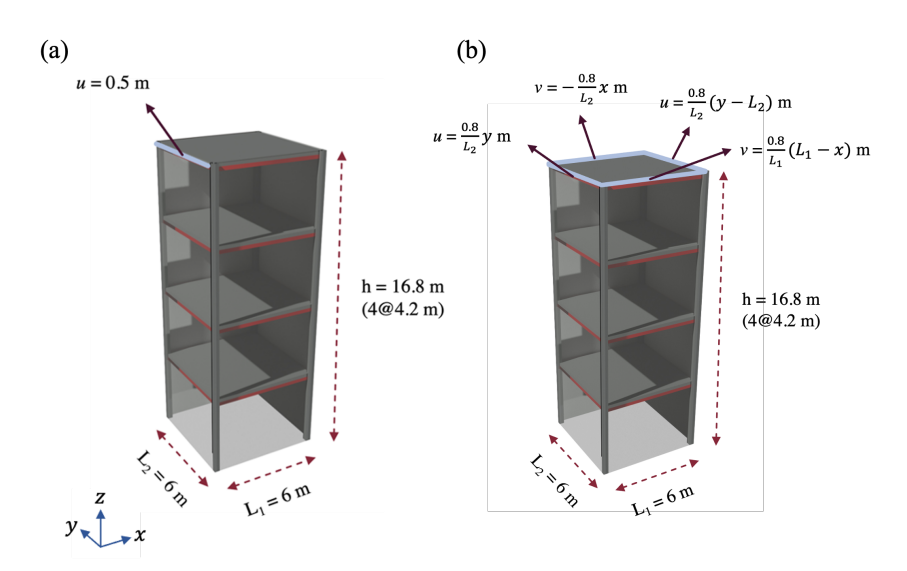


Figure 10: Schematic of a concrete shear core, featuring rigid connections to beams, columns, and the base. The core is subjected to different deformation fields: (a) lateral and (b) torsional displacements, both applied at the top floor.

4.2. Building core system

Core systems, for example, concrete shear cores located typically at the center of the structure, are used to resist lateral loads in buildings. Here we study the response of a 4-story concrete shear core system, shown in Fig. 10, with rigid connections to beams, columns and the base. The core system is analyzed under two load conditions: (i) lateral and (ii) torsional displacements at the top, as indicated in Figures 10(a) and (b). The domain of the core is discretized via a regular lattice of size 0.3m. Analogous to the previous example, an equally resolved finite element model is used for comparison.

Degrees of freedom	и	υ	w	R_{x}	R_y	R_z
Maximum relative error (%)	2.77	5.54	4.55	5.05	3.51	6.02

Table 4: Maximum relative error in displacements and rotations for core wall system subjected to lateral displacement

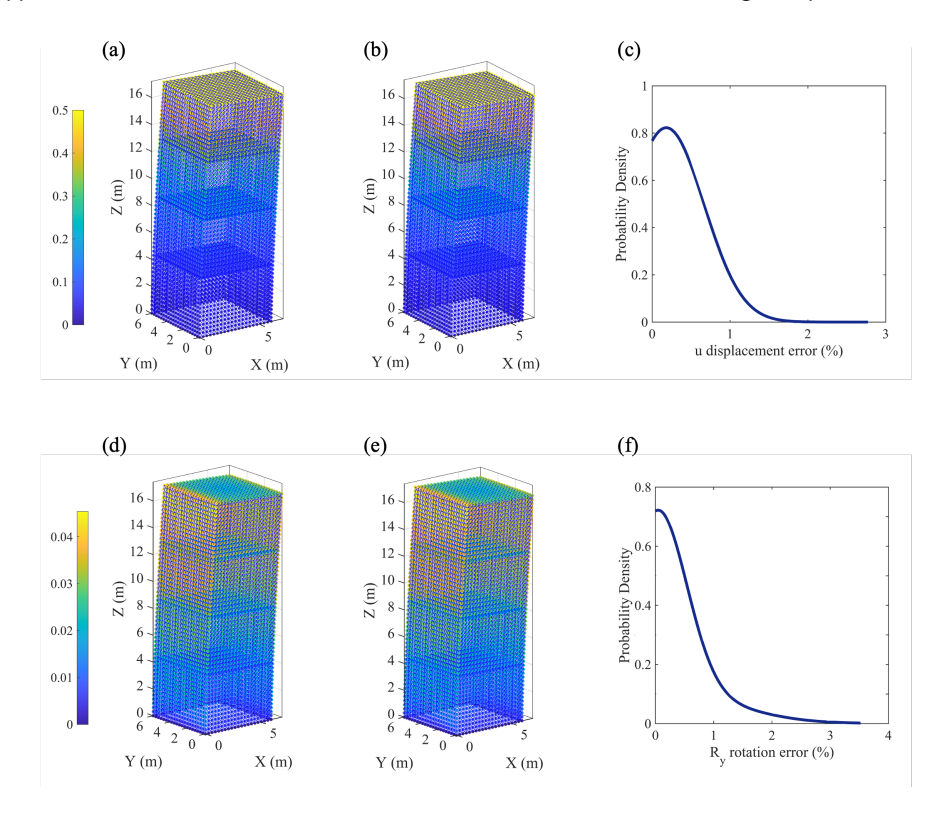


Figure 11: Comparative evaluation of PMF-based LEM results and finite element analysis for the concrete shear core system subjected to lateral displacement is shown in Fig. 10(a). The system is discretized using a lattice of size $a_0 = 0.3$ m. (a) and (b) present displacement u, obtained from PMF-based LEM and FEM simulations, respectively. whereas (d) and (e) show the rotation R_y . Figures (c,f) are the probability density functions of the relative error for u and R_y . The 95-percentile of the errors for u and u0 are 1.43% and 1.71%, respectively, signifying a high degree of consistency between the two approaches.

The results for the lateral loading condition are illustrated in Fig. 11 for the two significant displacement components u and R_y . We observe a close agreement between the deformation fields obtained via LEM and finite element analysis. The probability density functions of the relative errors shown in the left column of the figure indicate high accuracy of the results, with the 95-percentile of the relative errors at 1.43% for u and 1.71% for R_y .

The maximum relative errors for the displacements at all degrees of freedom are reported in Table 4. While the resolution of the discretization is identical to that of the framed structure in the previous example, we observe larger values for the relative error for different responses. This increase in error is attributed to the fact that the shear walls perpendicular to the loading direction exhibit out-of-plane deformations that require a higher resolution discretization to properly capture. We also examine the behavior of the same core system subject to a prescribed torsional displacement at the top, as illustrated in Figure 10(b). The applied displacement induces identical responses in x and y directions, one of which (e.g., u in x direction) is presented here. Figure 12 illustrates the displacement u and rotation R_z obtained via the LEM and compares them with the result of finite element analysis. The 95-percentile of the errors is 1.72% and 1.83% for u and R_z respectively, again indicating the promise of the PMF-based LEM in accurately capturing the response of an assembly of two-dimensional members.

4.3. Multi-story building with a core system

In our final example, we examine the response of a structural system that is a combination of the above two systems, namely a coupled system of frame and core. The structure is a four-story building with moment-resisting frames along the x and y axes, coupled with a shear core,both acting as lateral-load resisting components, and floors. The 1D and 2D components are discretized via a lattice of size $a_0 = 0.3m$ leading to the total of 65120 particles, and the building is subjected to a lateral displacement u = 0.5m in x direction on the top floor, as shown in Fig. 13.

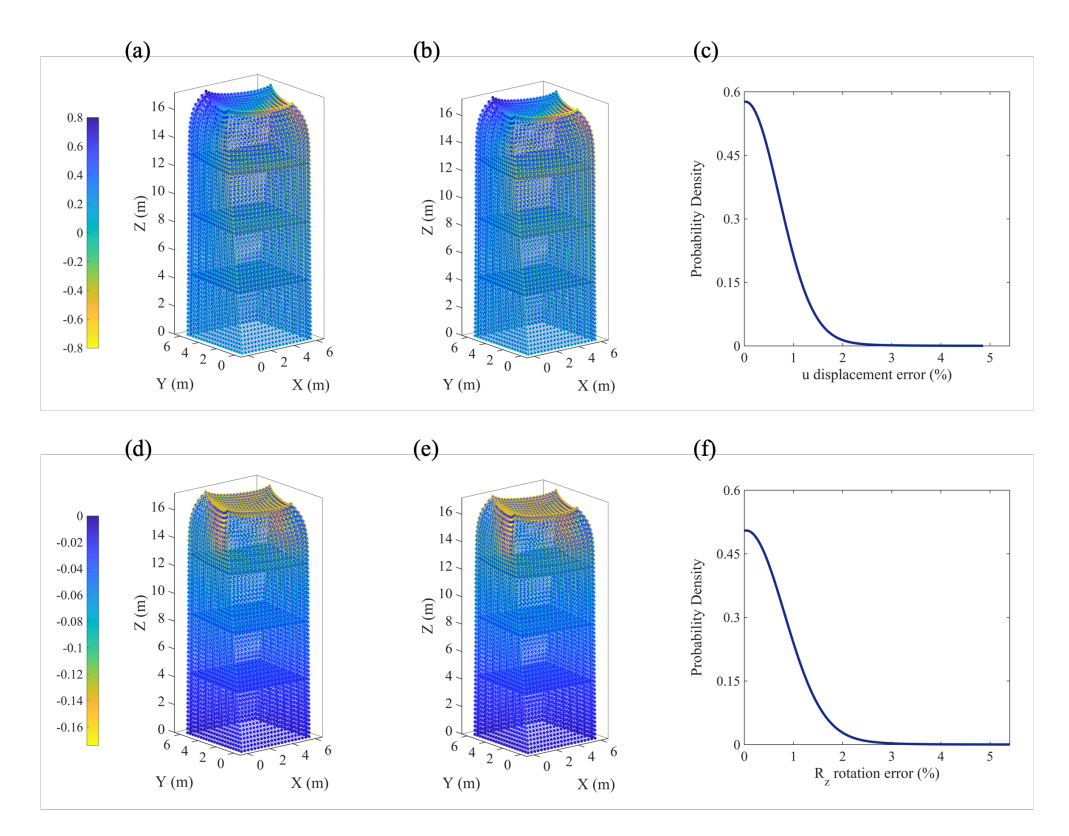


Figure 12: The results of PMF-based LEM and finite element analysis are compared for the concrete shear core system under torsional displacement at the top, as shown in Fig. 10(b). The lattice discretization of size $a_0 = 0.3$ m is utilized. In figures (a) and (b), the u displacement in the x direction obtained from PMF-based LEM and FEM simulations are depicted, whereas (d) and (e) provide the rotation around the z axis (R_z). The figures (c,f) illustrate the probability density function of the relative error for the u displacement and R_z rotation, respectively. The 95-percentile errors, standing at 1.72% for displacement u and 1.83% for rotation R_z , underline the accuracy of PMF-based LEM in predicting the behavior of the core system.

Fig. 14 compares the magnitudes of displacements u and R_y obtained via PMF-based LEM with those obtained via finite element analysis. Analogous to the previous examples, the results are in close agreement at almost every lattice particle. Fig. 14(g) shows the plot of the relative error in u within a section cut in the x direction, whereas Fig. 14(h) illustrates the relative error in R_y within a section cut in the y direction. As observed in these two error plots, large relative error magnitudes correspond to particles with insignificant displacement components. More specifically, we observe large relative errors in displacement u in the bottom of the shear wall of the first floor where u approaches zero. Similarly, the maximum error for rotation R_y occurs in the mid-span of the frame along the y direction with close to zero rotations. The probability density function of the relative errors shown in Figs. 14c and f also indicate the accuracy of the LEM results, with 95-percentile of errors at 0.79% and 0.71% for u and R_y respectively.

5. Concluding remarks

We proposed a simulation framework based on Lattice Element Method (LEM) for modeling the response of structures that provides a middle-ground solution between intricate FE models on one hand and overly simplistic multi-degree-of-freedom models on the other. The proposed framework draws on the potential of mean force approach to LEM, widely used in modeling fracture and damage in heterogeneous materials, and uses member- and component-level calibrated interaction potentials to model structural and non-structural elements as a collection of interacting nodes and bonds. The details needed for adaptation to modeling of building systems were laid out. This included calibration strategies for the determination of parameters of interaction potentials based on energy equivalency

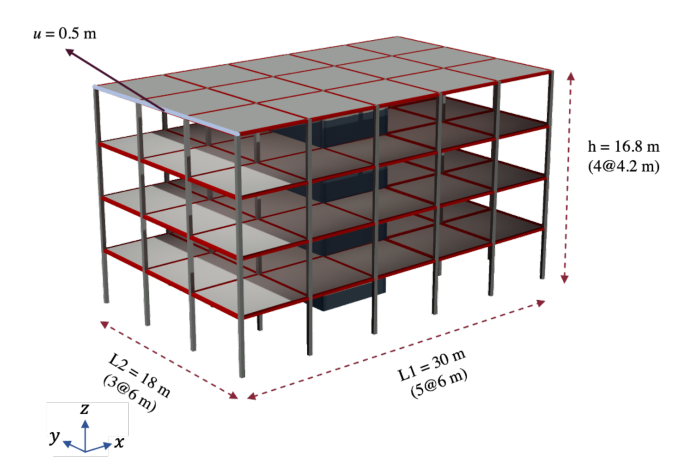


Figure 13: Schematic of a four-story concrete building comprised of moment-resisting frames along the x and y axes and a shear core, both functioning as lateral-load resisting components. The building is subjected to a lateral displacement u = 0.5m in the x direction on the top floor.

arguments for the lattice models of structural members and their continuum counterparts. We considered both 1D structural members (beams, columns, etc.) and 2D structural members (load-bearing walls, partitions, floors, etc.) under in-plane and out-of-plane actions. It was demonstrated that as the lattice discretization resolution increases, the in-plane and out-of-plane responses converge to those of the continuum models, but the resolution required for convergence for in-plane deformations is significantly lower than that needed for convergence for out-of-plane deformations.

The accuracy and effectiveness of the proposed framework were examined through analysing a set of building systems with different levels of complexity and comparison with the results of finite element simulations, indicating a close agreement between the results of the two methods with a similar discretization resolution and under various loading conditions.

While the development in this paper was limited to the linear regime, the prospects of leveraging a broad range of effective interaction potentials and the discrete nature of the proposed framework, along with energy-based failure criteria, are expected to enable modeling of nonlinear behavior and damage in structural and nonstructural members. It is further expected that LEM, as a quasi-static approach that relies on the minimum potential energy theorem, is amenable to studying dynamic problems through consideration of the system's potential and kinetic energies and satisfying the Euler-Lagrange equation. The proposed framework, therefore, has the potential to serve as (the basis for) an effective tool for evaluating the functional integrity and overall performance of building systems post-extreme events.

Acknowledgements

The authors would like to acknowledge the funding from United States National Science Foundation grants CMMI-1826155 and CMMI-2047832, and Office of Naval Research grant N00014-20-1-2849 (through MUST program at UMassD), as well as the support from College of Engineering and the Center for Scientific Computing and Data science Research (CSCDR) at the University of Massachusetts Dartmouth.

Declaration of competing interest

The authors declare that they have no known competing financial interests or personal relationships that could have appeared to influence the work reported in this paper.

Appendix I. Expansion of Lattice Stiffness Matrix

The total internal energy of the lattice bond ij can be expressed as the matrix form in Eq.8. Incorporating the contributions of stretch, bending, and torsional energy, the K_{ij} matrix is decomposed into K_{ij}^S , K_{ij}^B and K_{ij}^T :

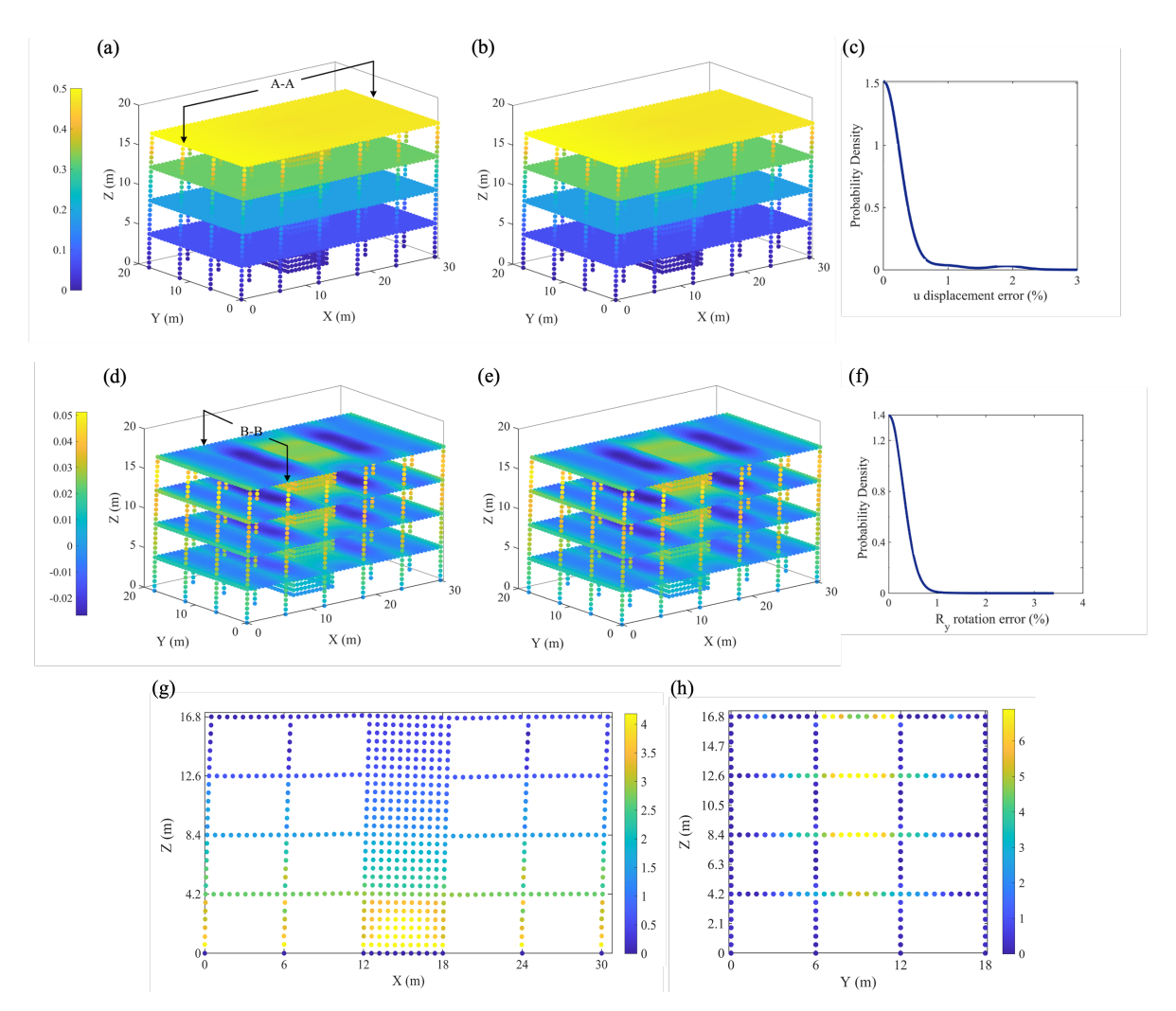


Figure 14: Comparison of the results of PMF-based LEM and finite element analysis for the concrete building shown in Fig. 13 with lattice discretization of size $a_0=0.3\mathrm{m}$. (a) and (b) show the displacement component u obtained, respectively, via PMF-based LEM and FEM simulations, while (d) and (e) present the rotation R_y . Figures (c) and (f) illustrate the probability density functions of the relative error for u and u a

$$K_{ij} = K_{ij}^S + K_{ij}^B + K_{ij}^T; (15)$$

The stiffness matrix K_{ij} can be expanded to:

$$K_{ij} = \frac{1}{2L^2} \begin{bmatrix} 2\epsilon_{ij}^S & 0 & 0 & 0 & 0 & 0 & -2\epsilon_{ij}^S & 0 & 0 & 0 & 0 & 0 \\ 0 & 2\epsilon_{ij}^{B,t} & 0 & 0 & 0 & L\epsilon_{ij}^{B,t} & 0 & -2\epsilon_{ij}^{B,t} & 0 & 0 & 0 & L\epsilon_{ij}^{B,t} \\ 0 & 0 & 2\epsilon_{ij}^{B,b} & 0 & -L\epsilon_{ij}^{B,b} & 0 & 0 & 0 & -2\epsilon_{ij}^{B,b} & 0 & -L\epsilon_{ij}^{B,b} & 0 \\ 0 & 0 & 0 & 2L^2\epsilon_{ij}^T & 0 & 0 & 0 & 0 & 0 & -2L^2\epsilon_{ij}^T & 0 & 0 \\ 0 & 0 & -L\epsilon_{ij}^{B,b} & 0 & k_{5,5} & 0 & 0 & 0 & L\epsilon_{ij}^{B,b} & 0 & k_{5,11} & 0 \\ 0 & L\epsilon_{ij}^{B,t} & 0 & 0 & 0 & k_{6,6} & 0 & -L\epsilon_{ij}^{B,t} & 0 & 0 & 0 & k_{6,12} \\ -2\epsilon_{ij}^S & 0 & 0 & 0 & 0 & 0 & 2\epsilon_{ij}^S & 0 & 0 & 0 & 0 & 0 \\ 0 & -2\epsilon_{ij}^{B,t} & 0 & 0 & 0 & -L\epsilon_{ij}^{B,t} & 0 & 2\epsilon_{ij}^{B,t} & 0 & 0 & 0 & -L\epsilon_{ij}^{B,t} \\ 0 & 0 & -2\epsilon_{ij}^{B,b} & 0 & L\epsilon_{ij}^{B,b} & 0 & 0 & 0 & 2\epsilon_{ij}^{B,t} & 0 & L\epsilon_{ij}^{B,b} & 0 \\ 0 & 0 & -2L^2\epsilon_{ij}^T & 0 & 0 & 0 & 0 & 2\epsilon_{ij}^{B,t} & 0 & L\epsilon_{ij}^{B,b} & 0 \\ 0 & 0 & -L\epsilon_{ij}^{B,b} & 0 & k_{11,5} & 0 & 0 & 0 & L\epsilon_{ij}^{B,b} & 0 & k_{11,11} & 0 \\ 0 & L\epsilon_{ij}^{B,t} & 0 & 0 & 0 & k_{12,6} & 0 & -L\epsilon_{ij}^{B,t} & 0 & 0 & 0 & k_{12,12} \end{bmatrix}$$

$$k_{5,5} = k_{11,11} = \frac{2}{3} L^2 (\epsilon_{ij}^{B,b} + 3\hat{\epsilon}_{ij}^{B,b}) \qquad k_{6,6} = k_{12,12} = \frac{2}{3} L^2 (\epsilon_{ij}^{B,t} + 3\hat{\epsilon}_{ij}^{B,t})$$

$$k_{5,11} = k_{11,5} = -\frac{1}{3} L^2 (5\epsilon_{ij}^{B,b} + 6\hat{\epsilon}_{ij}^{B,b}) \qquad k_{6,12} = k_{12,6} = \frac{1}{3} L^2 (\epsilon_{ij}^{B,t} - 6\hat{\epsilon}_{ij}^{B,t})$$

$$(16)$$

Appendix II. Transformation from Global to Local System of Coordinates

The following matrices are used to transform the deformation field from the global coordinate system (x, y, z) to the lattice coordinate system (n, b, t) according to equation 10:

$$Q^{n} = \begin{bmatrix} 1 & 0 & \sqrt{2}/2 & -\sqrt{2}/2 & -1 & 0 & -\sqrt{2}/2 & \sqrt{2}/2 \\ 0 & 1 & \sqrt{2}/2 & -\sqrt{2}/2 & 0 & -1 & -\sqrt{2}/2 & -\sqrt{2}/2 \\ 0 & 0 & 0 & 0 & 0 & 0 & 0 \end{bmatrix}$$
 (17)

References

- [1] A. B. Smith, 2020 u.s. billion-dollar weather and climate disasters, https://www.climate.gov/disasters2020 (2021).
- [2] M. Mahendran, C. Moor, Three-dimensional modeling of steel portal frame buildings, Journal of Structural Engineering 125 (8) (1999) 870–878.
- [3] B. Li, G. L. Hutchinson, C. F. Duffield, Contribution of typical non-structural components to the performance of high-rise buildings based on field reconnaissance, Journal of Building Appraisal 6 (2) (2010) 129–151.
- [4] B. Li, Enhancement of Structural Analysis of Multi-storey Buildings by Integrating Non-structural Components into Structural System, University of Melbourne, Department of Civil and Environmental Engineering, 2010.
- [5] P. Agarwal, M. Shrikhande, Earthquake resistant design of structures, phi learning pvt, Ltd., New Delhi (2006).
- [6] T. L. Karavasilis, C.-Y. Seo, Seismic structural and non-structural performance evaluation of highly damped self-centering and conventional systems, Engineering Structures 33 (8) (2011) 2248–2258.
- [7] Y. Li, B. R. Ellingwood, Hurricane damage to residential construction in the us: Importance of uncertainty modeling in risk assessment, Engineering structures 28 (7) (2006) 1009–1018.
- [8] V. Terzic, P. K. Villanueva, D. Saldana, D. Y. Yoo, Framework for modelling post-earthquake functional recovery of buildings, Engineering Structures 246 (2021) 113074.
- [9] X. Wang, H. Ebrahimian, R. Astroza, J. P. Conte, J. I. Restrepo, T. C. Hutchinson, Shake table testing of a full-scale five-story building: pre-test simulation of the test building and development of an ncs design criteria, in: Proc., 2013 ASCE Structures Congress, 2013.

Application of Mean Force Potential Lattice Element Method to Modeling Complex Structures

- [10] G. Bian, D. Padilla-Llano, J. Leng, S. Buonopane, C. Moen, B. Schafer, Opensees modeling of cold-formed steel framed wall system, in: Proceedings of 8th International Conference on Behavior of Steel Structures in Seismic Areas, 2015.
- [11] F. Scozzese, G. Terracciano, A. Zona, G. Della Corte, A. Dall'Asta, R. Landolfo, Analysis of seismic non-structural damage in single-storey industrial steel buildings, Soil Dynamics and Earthquake Engineering 114 (2018) 505–519.
- [12] G. Gabbianelli, D. Perrone, E. Brunesi, R. Monteiro, Seismic acceleration and displacement demand profiles of non-structural elements in hospital buildings, Buildings 10 (12) (2020) 243.
- [13] P. M. Calvi, Relative displacement floor spectra for seismic design of non structural elements, Journal of Earthquake Engineering 18 (7) (2014) 1037–1059.
- [14] I. Koutromanos, A. Stavridis, P. B. Shing, K. Willam, Numerical modeling of masonry-infilled rc frames subjected to seismic loads, Computers & Structures 89 (11-12) (2011) 1026–1037.
- [15] N. Aravas, R. McMeeking, Finite element analysis of void growth near a blunting crack tip, Journal of the Mechanics and Physics of Solids 33 (1) (1985) 25–49.
- [16] P. Charalambides, R. McMeeking, Finite element method simulation of crack propagation in a brittle microcracking solid, Mechanics of Materials 6 (1) (1987) 71–87.
- [17] F. A. Pires, E. de Souza Neto, D. Owen, On the finite element prediction of damage growth and fracture initiation in finitely deforming ductile materials, Computer Methods in Applied Mechanics and Engineering 193 (48-51) (2004) 5223–5256.
- [18] I. Babuška, W. C. Rheinboldt, A-posteriori error estimates for the finite element method, International Journal for Numerical Methods in Engineering 12 (10) (1978) 1597–1615.
- [19] O. C. Zienkiewicz, J. Z. Zhu, A simple error estimator and adaptive procedure for practical engineering analysis, International journal for numerical methods in engineering 24 (2) (1987) 337–357.
- [20] S. Benzley, Representation of singularities with isoparametric finite elements, International journal for numerical methods in engineering 8 (3) (1974) 537–545.
- [21] T. Belytschko, T. Black, Elastic crack growth in finite elements with minimal remeshing, International journal for numerical methods in engineering 45 (5) (1999) 601–620.
- [22] N. Moës, J. Dolbow, T. Belytschko, A finite element method for crack growth without remeshing, International journal for numerical methods in engineering 46 (1) (1999) 131–150.
- [23] J. Oliver, A. E. Huespe, P. J. Sánchez, A comparative study on finite elements for capturing strong discontinuities: E-fem vs x-fem, Computer methods in applied mechanics and engineering 195 (37-40) (2006) 4732–4752.
- [24] H. Talebi, M. Silani, S. P. Bordas, P. Kerfriden, T. Rabczuk, A computational library for multiscale modeling of material failure, Computational Mechanics 53 (2014) 1047–1071.
- [25] N. Sukumar, J. Dolbow, N. Moës, Extended finite element method in computational fracture mechanics: a retrospective examination, International Journal of Fracture 196 (1) (2015) 189–206.
- [26] X.-e. Wang, J. Yang, Q.-f. Liu, Y.-m. Zhang, C. Zhao, A comparative study of numerical modelling techniques for the fracture of brittle materials with specific reference to glass, Engineering Structures 152 (2017) 493–505.
- [27] A. Shojaei, T. Mudric, M. Zaccariotto, U. Galvanetto, A coupled meshless finite point/peridynamic method for 2d dynamic fracture analysis, International Journal of Mechanical Sciences 119 (2016) 419–431.
- [28] M. N. Nguyen, T. Q. Bui, N. T. Nguyen, T. T. Truong, et al., Simulation of dynamic and static thermoelastic fracture problems by extended nodal gradient finite elements, International Journal of Mechanical Sciences 134 (2017) 370–386.
- [29] L. Dormieux, A. Molinari, D. Kondo, Micromechanical approach to the behavior of poroelastic materials, Journal of the Mechanics and Physics of Solids 50 (10) (2002) 2203–2231.
- [30] J. G. Van Mier, Multi-scale interaction potentials (f- r) for describing fracture of brittle disordered materials like cement and concrete, International Journal of Fracture 143 (1) (2007) 41–78.
- [31] G. F. de Medeiros, A. S. Milani, A. Lubeck, G. Mohamad, R. Q. Rodriguez, L. E. Kosteski, Numerical analysis of masonry walls with horizontal chases using the lattice discrete element method (Idem), Engineering Structures 253 (2022) 113647.
- [32] M. Ghajari, L. Iannucci, P. Curtis, A peridynamic material model for the analysis of dynamic crack propagation in orthotropic media, Computer Methods in Applied Mechanics and Engineering 276 (2014) 431–452.
- [33] A. Truszkowska, Q. Yu, P. A. Greaney, T. M. Evans, J. J. Kruzic, A discrete element method representation of an anisotropic elastic continuum, Journal of the Mechanics and Physics of Solids 121 (2018) 363–386.
- [34] A. S. Fallah, I. N. Giannakeas, R. Mella, M. R. Wenman, Y. Safa, H. Bahai, On the computational derivation of bond-based peridynamic stress tensor, Journal of Peridynamics and Nonlocal Modeling 2 (2020) 352–378.
- [35] P. A. Cundall, O. D. Strack, A discrete numerical model for granular assemblies, geotechnique 29 (1) (1979) 47–65.
- [36] J. Ghaboussi, R. Barbosa, Three-dimensional discrete element method for granular materials, International Journal for Numerical and Analytical Methods in Geomechanics 14 (7) (1990) 451–472.
- [37] P. Cleary, Modelling comminution devices using dem, International Journal for numerical and analytical methods in geomechanics 25 (1) (2001) 83–105.
- [38] H.-b. Du, F. Dai, Y. Xu, Z. Yan, M.-d. Wei, Mechanical responses and failure mechanism of hydrostatically pressurized rocks under combined compression-shear impacting, International Journal of Mechanical Sciences 165 (2020) 105219.
- [39] H. Fu, S. Kaewunruen, Experimental and dem investigation of axially-loaded behaviours of iwp-based structures, International Journal of Mechanical Sciences 235 (2022) 107738.
- [40] D. Sulsky, Z. Chen, H. L. Schreyer, A particle method for history-dependent materials, Computer methods in applied mechanics and engineering 118 (1-2) (1994) 179–196.
- [41] J. A. Nairn, Material point method calculations with explicit cracks, Computer Modeling in Engineering and Sciences 4 (6) (2003) 649-664.

Application of Mean Force Potential Lattice Element Method to Modeling Complex Structures

- [42] Y. Guo, J. Nairn, Three-dimensional dynamic fracture analysis using the material point method, Computer Modeling in Engineering and Sciences 16 (3) (2006) 141.
- [43] T. Kawai, New element models in discrete structural analysis, Journal of the Society of Naval Architects of Japan 1977 (141) (1977) 174–180.
- [44] J. E. Bolander Jr, S. Berton, Simulation of shrinkage induced cracking in cement composite overlays, Cement and Concrete Composites 26 (7) (2004) 861–871.
- [45] M. Kunieda, H. Ogura, N. Ueda, H. Nakamura, Tensile fracture process of strain hardening cementitious composites by means of three-dimensional meso-scale analysis, Cement and Concrete Composites 33 (9) (2011) 956–965.
- [46] E. Schlangen, E. J. Garboczi, Fracture simulations of concrete using lattice models: computational aspects, Engineering fracture mechanics 57 (2-3) (1997) 319–332.
- [47] V. Topin, J.-Y. Delenne, F. Radjaı, L. Brendel, F. Mabille, Strength and failure of cemented granular matter, The European Physical Journal E 23 (4) (2007) 413–429.
- [48] M. Nikolić, X. N. Do, A. Ibrahimbegovic, Ž. Nikolić, Crack propagation in dynamics by embedded strong discontinuity approach: Enhanced solid versus discrete lattice model, Computer Methods in Applied Mechanics and Engineering 340 (2018) 480–499.
- [49] R. Affes, J.-Y. Delenne, Y. Monerie, F. Radjai, V. Topin, Tensile strength and fracture of cemented granular aggregates, The European Physical Journal E 35 (11) (2012) 117.
- [50] M. Ostoja-Starzewski, P. Sheng, K. Alzebdeh, Spring network models in elasticity and fracture of composites and polycrystals, Computational Materials Science 7 (1-2) (1996) 82–93.
- [51] H. J. Herrmann, Introduction to modern ideas on tracture patterns, in: Random Fluctuations and Pattern Growth: Experiments and Models, Springer, 1988, pp. 149–160.
- [52] V. Topin, J.-Y. Delenne, F. Radjai, Lattice element method, Laboratoire de M'ecanique et G'enie Civil, CNRS-Universit'e Montpellier 2.
- [53] J. E. Bolander, J. Eliáš, G. Cusatis, K. Nagai, Discrete mechanical models of concrete fracture, Engineering Fracture Mechanics 257 (2021) 108030
- [54] P. Grassl, A. Antonelli, 3d network modelling of fracture processes in fibre-reinforced geomaterials, International Journal of Solids and Structures 156 (2019) 234–242.
- [55] J. Wang, Development and application of a micromechanics-based numerical approach for the study of crack propagation in concrete, Tech. rep., EPFL (1994).
- [56] G. Lilliu, J. G. van Mier, 3d lattice type fracture model for concrete, Engineering Fracture Mechanics 70 (7-8) (2003) 927–941.
- [57] C. Moukarzel, H. Herrmann, A vectorizable random lattice, Journal of Statistical Physics 68 (5) (1992) 911–923.
- [58] J. Bolander, Y. Kobashi, Size effect mechanisms in numerical concrete fracture, Fracture mechanics of concrete structures, Aedificatio Publishers, Freiburg (1995) 535–542.
- [59] H. Laubie, F. Radjai, R. Pellenq, F.-J. Ulm, A potential-of-mean-force approach for fracture mechanics of heterogeneous materials using the lattice element method, Journal of the Mechanics and Physics of Solids 105 (2017) 116–130.
- [60] K. Ioannidou, K. J. Krakowiak, M. Bauchy, C. G. Hoover, E. Masoero, S. Yip, F.-J. Ulm, P. Levitz, R. J.-M. Pellenq, E. Del Gado, Mesoscale texture of cement hydrates, Proceedings of the National Academy of Sciences 113 (8) (2016) 2029–2034.
- [61] H. Zhu, A. J. Whittle, R. J.-M. Pellenq, Potential of mean force for face–face interactions between pairs of 2: 1 clay mineral platelets, Langmuir 38 (43) (2022) 13065–13074.
- [62] H. Laubie, S. Monfared, F. Radjaï, R. Pellenq, F.-J. Ulm, Effective potentials and elastic properties in the lattice-element method: isotropy and transverse isotropy, Journal of Nanomechanics and Micromechanics 7 (3) (2017) 04017007.
- [63] X. Wang, M. Botshekan, F.-J. Ulm, M. Tootkaboni, A. Louhghalam, A hybrid potential of mean force approach for simulation of fracture in heterogeneous media, Computer Methods in Applied Mechanics and Engineering 386 (2021) 114084.
- [64] X. Lu, Q. Cheng, Z. Xu, Y. Xu, C. Sun, Real-time city-scale time-history analysis and its application in resilience-oriented earthquake emergency responses, Applied Sciences 9 (17) (2019) 3497.
- [65] W. Elhaddad, F. McKenna, M. Rynge, J. Lowe, C. Wang, A. Zsarnoczay, Nheri-simcenter, WorkflowRegionalEarthquake: rWHALE (Version v1. 1.0) (2019).
- [66] E. Masoero, C. O'Shaughnessy, P. D. Gosling, B. M. Chiaia, Topology optimization using the discrete element method. part 2: Material nonlinearity, Meccanica 57 (6) (2022) 1233–1250.
- [67] P. M. Morse, Diatomic molecules according to the wave mechanics. ii. vibrational levels, Physical review 34 (1) (1929) 57.
- [68] A. Lee, T. Kalotas, N. Adams, Modified morse potential for diatomic molecules, Journal of molecular spectroscopy 191 (1) (1998) 137-141.
- [69] C. Avendano, T. Lafitte, A. Galindo, C. S. Adjiman, G. Jackson, E. A. Müller, Saft-γ force field for the simulation of molecular fluids. 1. a single-site coarse grained model of carbon dioxide, The Journal of Physical Chemistry B 115 (38) (2011) 11154–11169.
- [70] B. M. Chiaia, E. Masoero, Analogies between progressive collapse of structures and fracture of materials, International journal of fracture 154 (1-2) (2008) 177–193.
- [71] R. Qu, Z. Zhang, P. Zhang, Z. Liu, Z. Zhang, Generalized energy failure criterion, Scientific reports 6 (1) (2016) 23359.
- [72] Q. Li, Strain energy density failure criterion, International Journal of Solids and Structures 38 (38-39) (2001) 6997–7013.
- [73] K. Keremides, M. J. Abdolhosseini Qomi, R. J. Pellenq, F.-J. Ulm, Potential-of-mean-force approach for molecular dynamics—based resilience assessment of structures, Journal of Engineering Mechanics 144 (8) (2018) 04018066.
- [74] F. Ulm, K. Keremidis, R. Pellenq, M. Qomi, Molecular dynamics-based structural mechanics of buildings' resilience, in: Computational Modelling of Concrete Structures, CRC Press, 2018, pp. 3–13.
- [75] E. Schlangen, E. Garboczi, New method for simulating fracture using an elastically uniform random geometry lattice, International journal of engineering science 34 (10) (1996) 1131–1144.
- [76] M. Nikolić, E. Karavelić, A. Ibrahimbegovic, P. Miščević, Lattice element models and their peculiarities, Archives of Computational Methods in Engineering 25 (3) (2018) 753–784.
- [77] M. Ostoja-Starzewski, Lattice models in micromechanics, Appl. Mech. Rev. 55 (1) (2002) 35–60.

Application of Mean Force Potential Lattice Element Method to Modeling Complex Structures

[78]	J. Christoffersen,	, M. M. Mehrabadi,	S. Nemat-Nasser,	A micromechanical	description of gra	anular material behavior (1981).
------	--------------------	--------------------	------------------	-------------------	--------------------	----------------------------------

^[79] M. Deru, K. Field, D. Studer, K. Benne, B. Griffith, P. Torcellini, B. Liu, M. Halverson, D. Winiarski, M. Rosenberg, et al., Us department of energy commercial reference building models of the national building stock (2011).